

Effect of forward scattering and rigid top surface on the onset of phototactic bioconvection in an algal suspension illuminated by both oblique collimated and diffuse irradiation

S. K. Rajput^{1, a)}

Department of Mathematics, PDPM Indian Institute of Information Technology Design and Manufacturing, Jabalpur 482005, India.

The effect of the rigid top surface on the onset of phototactic bioconvection is investigated using linear stability theory for a suspension of forward-scattering phototactic algae in this article. The suspension is uniformly illuminated by both diffuse and oblique collimated flux. The nature of disturbance of bio-convective instability transits from a stationary (overstable) to an overstable (stationary) state as the forward scattering coefficient varies under fixed parameters. In presence of rigid top surface, the suspension becomes more stable as the forward scattering coefficient increases.

^{a)}Email: shubh.iitj@gmail.com

I. INTRODUCTION

A ubiquitous phenomenon of fluid dynamics which leads to patterns formation in a suspension of living microorganisms (such as algae, bacteria etc.) is defined as Bioconvection¹⁻⁵. Platt was the first who introduce the term bioconvection in 1961. In most cases, these living microorganisms have a greater density than the base fluid (water) on a small scale, and they swim collectively in an upward direction. But there are some cases available in a natural environment where there is no need for greater density and to float in an upward direction to form a biological pattern² Non-living microorganism does not show this type of behaviour (pattern formation). Microorganisms show a behavioural response in their swimming direction due to their body structure and external stimuli in the natural environment called taxes. Gravitaxis is due to gravitational acceleration; gyrotaxis occurs due to gravitational acceleration and viscous torque where microorganism are bottom heavy; phototaxis is movement of microorganisms towards or away from the illumination source. In this article, we discuss the effect of phototaxis only.

Studies on bioconvection patterns in algal suspensions have found that the interplay of diffuse and oblique collimated irradiation can affect the flow of fluids and concentration patterns of cells⁶⁻¹⁰. Under intense light condition, the bioconvective patterns may either remain unchanged or be disrupted. The response of algae to moderate or intense light is a critical factor in the changes seen in bioconvection patterns due to light intensity¹¹. Additionally, the absorption and scattering of light by microorganisms can also play an important role in the changes in bioconvective patterns¹². Algal light scattering can be categorized as isotropic or anisotropic, with the latter being further divided into forward and backward scattering based on cell size, shape, and refractive index. Due to their size, algae mainly scatter light in the forward direction in the visible wavelength range.

The bioconvective system is being studied using the phototaxis model proposed by Panda¹³, which involves illuminating a forward-scattering algal suspension with both diffuse and vertical collimated flux. In natural environments, algal suspensions are exposed to oblique collimated flux that can penetrate deeper waters and affect the radiation field, influencing the swimming behavior of algae and light intensity profiles. For realistic models of phototaxis for bioconvective instabilities should include both types of flux (oblique and diffuse). This paper investigates bioconvective instability in presence of both types of flux (oblique and diffuse).

This study focuses on the analysis of bioconvective instabilities in a dilute algal suspension.

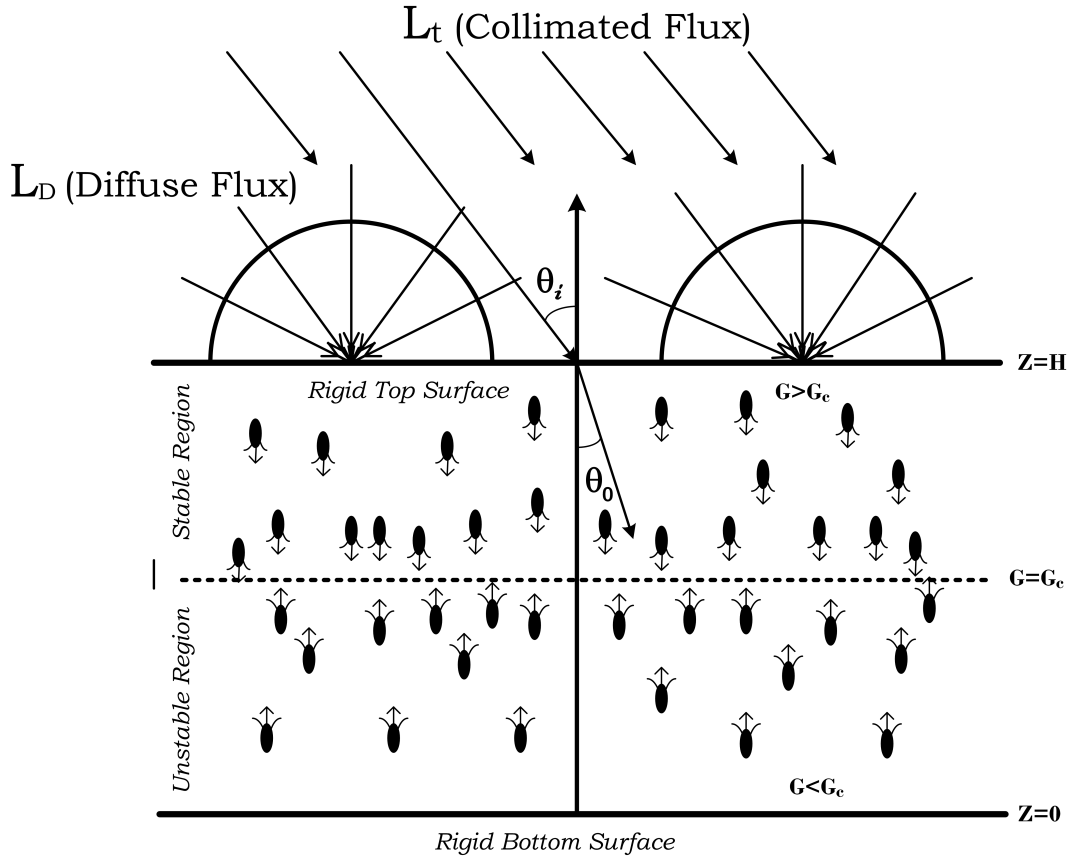


FIG. 1. Accumulation of algae cells as a sublayer at $G = G_c$, where G_c is critical intensity.

The equilibrium solution is obtained by considering the flow velocity is zero in the suspension. Under this condition, the balance between phototaxis and diffusion leads to a horizontal sublayer where cells accumulate, separating the suspension into two regions. The position of the sublayer is dependent on the critical intensity G_c . Above the sublayer ($G > G_c$), the intensity of light is high enough to suppress cell motion, while below it ($G < G_c$), cells move upwards towards the sublayer due to phototaxis. This sublayer divides the suspension into two regions based on G_c , with the unstable lower region capable of penetrating the stable upper region through fluid motions if the system becomes unstable, a phenomenon referred to as penetrative convection¹⁴.

Over the years, researchers have made significant progress in modeling phototactic bioconvection. For instance, Vincent and Hill¹⁵ studied the onset of phototactic bioconvection and discovered non-stationary and non-oscillatory modes of disturbance where the suspension. Ghorai and Hill¹⁶ simulated a two-dimensional bioconvective flow pattern using the model of Vincent and Hill¹⁵, but they neglected scattering by algae. Ghorai et al.¹⁷ studied the onset of bioconvection in

an isotropic scattering suspension and found a steady-state profile with a sublayer located at two different depths due to isotropic scattering by algae for certain parameters. Ghorai and Panda¹⁸ examined linear stability analysis in a forward scattering algal suspension and reported a transition from a non-oscillatory (non-stationary) to a non-stationary (non-oscillatory) mode at bioconvective instability due to forward scattering. In all these studies, the diffuse flux are not consider as an illuminating source. Panda *et al.*¹⁹ investigated the effect of diffuse flux on bioconvective instability isotropic scattering algal suspension and found an considerable stabilizing effect due to diffuse flux. After that, Panda¹³ proposed a model in which he studied the impact of both diffuse and vertical collimated flux and reported that stabilizing effect due to both diffuse collimated flux and forward scattering coefficient. However, these studies did not take into account the effects of oblique collimated flux. Panda *et al.*²⁰ incorporated oblique collimated flux and found that the bioconvective solutions switch from a non-oscillatory state to an overstable state and vice versa at bioconvective instability due to oblique collimated flux. Kumar²¹ investigated the impact of oblique collimated flux on bioconvective solutions in an isotropic scattering algal suspension and found that the bioconvection solutions become mostly oscillatory. After that Kumar²² explored the effect of rigid top and bottom surfaces. In this study, he reported a considerable stabilizing impact on the bio-convective instability caused by rigid surfaces. Panda and Rajput developed a model for a type of algae suspension that scatters light in all directions, and analyzed its stability under illumination by both diffuse and oblique collimated light. They found that the bio-convective solution can transition from non-oscillatory to oscillatory behavior for fixed parameters when subjected to oblique collimated flux. They later extended their analysis to include anisotropic scattering in the suspension and found that the forward scattering coefficient has a stabilizing effect on bioconvective instability. The authors note that further research is needed to examine the impact of both oblique collimated and diffuse light on phototactic bioconvection in a forward scattering algal suspension with rigid non-slip vertical boundaries. The current study aims to investigate the effects of these boundaries on the suspension using a realistic phototaxis model.

The article follows a structured approach. It starts with the mathematical formulation of the problem, followed by obtaining the equilibrium solution and perturbing the base bioconvective governing system by small disturbances. Next, the linear stability problem is derived and solved using numerical methods. Finally, the results of the model are presented and discussed.

II. MATHEMATICAL FORMULATION

The system being studied is a forward-scattering algal suspension occupying the region between two infinite parallel boundaries in the y - z plane, as depicted in Fig. 2. The upper surface of the suspension is uniformly illuminated by both oblique collimated and diffuse flux. The algae in the suspension absorb and scatter the incident light in the forward direction, which occurs due to the difference in the refractive index of the algae and water.

A. THE AVERAGE SWIMMING DIRECTION

The Radiative Transfer Equation (hereafter referred to as RTE) is used to calculate the light intensity which is given by

$$\frac{dL(\mathbf{x}, \mathbf{s})}{ds} + (a + \sigma_s)L(\mathbf{x}, \mathbf{s}) = \frac{\sigma_s}{4\pi} \int_0^{4\pi} L(\mathbf{x}, \mathbf{s}') \Xi(\mathbf{s}, \mathbf{s}') d\Omega', \quad (1)$$

where a , σ_s and Ω' are the absorption coefficient, scattering coefficients respectively. $\Xi(\mathbf{s}, \mathbf{s}')$ is the scattering phase function, which provides the angular distribution of the light intensity scattered from \mathbf{s}' direction into \mathbf{s} direction. Here, we assume that $\Xi(\mathbf{s}, \mathbf{s}')$ is linearly anisotropic with azimuthal symmetry $\Xi(\mathbf{s}, \mathbf{s}') = 1 + A_1 \cos \theta \cos \theta'$. Here, A_1 is the anisotropic coefficient. The anisotropic coefficient defines forward scattering for $0 < A_1 < 1$ and backward scattering for $-1 < A_1 < 0$. If consider the case $A_1 = 0$, it shows isotropic scattering.

The light intensity on the top of the suspension is given by

$$L(\mathbf{x}_H, \mathbf{s}) = L_t \delta(\mathbf{s} - \mathbf{s}_0) + \frac{L_D}{\pi} = L_t \delta(\cos \theta - \cos \theta_0) + \frac{L_D}{\pi},$$

where $\mathbf{x}_H = (x, y, H)$ is the location on the top boundary surface. Here, L_t and L_D are the magnitudes of collimated and diffuse irradiation respectively^{12,13}. Now consider $a = \alpha n(\mathbf{x})$ and $\sigma_s = \beta n(\mathbf{x})$, then the RTE becomes

$$\frac{dL(\mathbf{x}, \mathbf{s})}{ds} + (\alpha + \beta)nL(\mathbf{x}, \mathbf{s}) = \frac{\beta n}{4\pi} \int_0^{4\pi} L(\mathbf{x}, \mathbf{s}') (A_1 \cos \theta \cos \theta') d\Omega'. \quad (2)$$

In the medium, the total intensity at a fixed point \mathbf{x} is

$$G(\mathbf{x}) = \int_0^{4\pi} L(\mathbf{x}, \mathbf{s}) d\Omega,$$

and the radiative heat flux is given by

$$\mathbf{q}(\mathbf{x}) = \int_0^{4\pi} L(\mathbf{x}, \mathbf{s}) \mathbf{s} d\Omega. \quad (3)$$

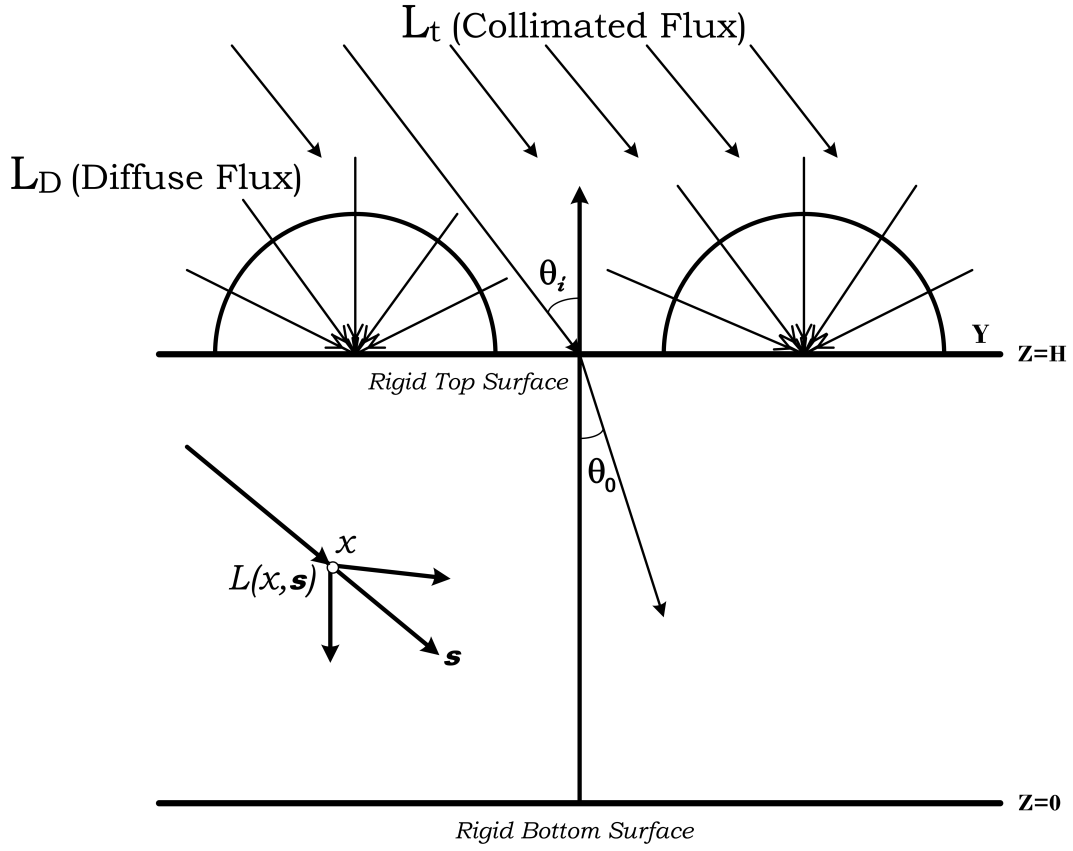


FIG. 2. Geometric configuration of the problem.

The mean swimming velocity of cell is given by

$$\mathbf{W}_c = W_c \langle \mathbf{p} \rangle,$$

where W_c is the average cell swimming speed and $\langle \mathbf{p} \rangle$ is cell's mean swimming orientation, which is calculated by

$$\langle \mathbf{p} \rangle = -M(G) \frac{\mathbf{q}}{|\mathbf{q}|}, \quad (4)$$

where $M(G)$, is the taxis response function (taxis function), which shows the response of algae cells to light and has the mathematical form such that

$$M(G) = \begin{cases} \geq 0, & \text{if } G(\mathbf{x}) \leq G_c, \\ < 0, & \text{if } G(\mathbf{x}) > G_c. \end{cases}$$

The mean swimming direction becomes zero at the critical light intensity ($G = G_c$). Generally, the exact functional form of taxis function depends on the species of the microorganisms¹⁵.

B. GOVERNING EQUATIONS WITH THE SPECIFIC BOUNDARY CONDITIONS

Consider a suspension of phototactic microorganisms with average fluid velocity U and n number of algal cells in unit volume. In the algal suspension all cells have constant physical properties like volume V and density $\rho + \Delta\rho$, where ρ is the density of water ($\Delta\rho/\rho \ll 1$) except for the buoyancy force. Let the suspension be incompressible. Then the system of equations of this model is defined as follows:

Continuity equation

$$\nabla \cdot U = 0. \quad (5)$$

The momentum equation under the Boussinesq approximation

$$\rho \frac{DU}{Dt} = -\nabla P + \mu \nabla^2 U - ngV\Delta\rho \hat{z}, \quad (6)$$

where P is dynamic pressure, μ is the dynamic viscosity of the suspension which is assumed to be that of fluid.

Cell conservation equation

$$\frac{\partial n}{\partial t} = -\nabla \cdot B, \quad (7)$$

where B is the total cell flux which is given by

$$B = nU + nW_c \langle p \rangle - D\nabla n. \quad (8)$$

Here, cell diffusivity D is assumed to be constant, with the result that $D = DI$. Two key assumptions are considered that help to remove Fokker-Plank equation from the governing equation similar to the Panda.¹³

Here, lower and upper boundaries are considered rigid and impermeable. Hence, at the boundaries, no fluid flow and no cell movement through the boundaries. The condition of rigid no slip and zero flux are defined as

$$U \times \hat{z} = 0 \quad \text{on } z = 0, H. \quad (9)$$

$$B \cdot \hat{z} = 0 \quad \text{on } z = 0, H. \quad (10)$$

We make the assumption that the upper boundary is subjected to oblique and diffuse irradiation uniformly. This leads to a specific set of conditions for the intensity at the boundaries, which are as follows

$$L(x, y, z = 0, \theta, \phi) = L_t \delta(s - s_0) + \frac{L_D}{\pi}, \quad (\pi/2 \leq \theta \leq \pi), \quad (11a)$$

$$L(x, y, z = 0, \theta, \phi) = 0, \quad (0 \leq \theta \leq \pi/2). \quad (11b)$$

C. NON DIMENSIONLIZATION OF THE GOVERNING EQUATIONS

To express the governing equations without dimensions, certain scales are selected. These include H for length, H^2/D for time, D/H for velocity, $\mu D/H^2$ for pressure, and \bar{n} for concentration. As a result, the governing equations can be represented in a dimensionless form

$$\nabla \cdot \mathbf{U} = 0, \quad (12)$$

$$S_c^{-1} \left(\frac{D\mathbf{U}}{Dt} \right) = -\nabla P_e - Rn\hat{z} + \nabla^2 \mathbf{U}, \quad (13)$$

$$\frac{\partial n}{\partial t} = -\nabla \cdot \mathbf{B}, \quad (14)$$

where

$$\mathbf{B} = n(\mathbf{U} + V_c \langle \mathbf{p} \rangle) - \nabla n. \quad (15)$$

In the given equations, the parameter S_c is defined as the ratio of viscosity (μ) and diffusion coefficient (D). The scaled swimming speed is represented by $V_c = W_c H/D$. Additionally, the Rayleigh number R is introduced as a controlling parameter, and is defined as $R = \bar{n} V g \delta \rho H^3 / \mu D$.

The boundary conditions can also be represented in a dimensionless form as

$$\mathbf{U} \times \hat{z} = 0 \quad \text{on} \quad z = 0, 1. \quad (16)$$

$$\mathbf{B} \cdot \hat{z} = 0 \quad \text{on} \quad z = 0, 1. \quad (17)$$

Nondimensional Radiative Transfer Equation (RTE) is

$$\frac{dL(\mathbf{x}, \mathbf{s})}{ds} + \tau_H n L(\mathbf{x}, \mathbf{s}) = \frac{\sigma n}{4\pi} \int_0^{4\pi} L(\mathbf{x}, \mathbf{s}') (A_1 \cos \theta \cos \theta') d\Omega', \quad (18)$$

where $\tau_H = (\alpha + \beta) \bar{n} H$, $\sigma = \beta \bar{n} H$ are the non-dimensional extinction coefficient and scattering coefficient respectively. The scattering albedo $\omega = \sigma / (\tau_H + \sigma)$ measures the scattering efficiency of microorganisms. In terms of scattering albedo ω , Eq. (18) can be written as

$$\frac{dL(\mathbf{x}, \mathbf{s})}{ds} + \tau_H n L(\mathbf{x}, \mathbf{s}) = \frac{\omega \tau_H n}{4\pi} \int_0^{4\pi} L(\mathbf{x}, \mathbf{s}') (A_1 \cos \theta \cos \theta') d\Omega'. \quad (19)$$

The value of the scattering albedo ω ranges from 0 to 1, where $\omega = 1$ represents a medium that purely scatters light, and $\omega = 0$ represents a medium that purely absorbs light. The RTE can also be expressed in terms of direction cosine as

$$\xi \frac{dL}{dx} + \eta \frac{dL}{dy} + \nu \frac{dL}{dz} + \tau_H n L(\mathbf{x}, \mathbf{s}) = \frac{\omega \tau_H n}{4\pi} \int_0^{4\pi} L(\mathbf{x}, \mathbf{s}') (A_1 \cos \theta \cos \theta') d\Omega', \quad (20)$$

In the dimensionless form, the intensity at the boundaries is given by

$$L(x, y, z = 1, \theta, \phi) = L_t \delta(s - s_0) + \frac{L_D}{\pi}, \quad (\pi/2 \leq \theta \leq \pi), \quad (21a)$$

$$L(x, y, z = 0, \theta, \phi) = 0, \quad (0 \leq \theta \leq \pi/2). \quad (21b)$$

III. THE BASIC (EQUILIBRIUM) STATE SOLUTION

Equations (12) – (14) and (20) possess a solution at equilibrium that can be expressed as

$$U = 0, \quad n = n_s(z) \quad \text{and} \quad L = L_s(z, \theta). \quad (22)$$

Hence, at the equilibrium state, the total intensity and radiative flux can be expressed as

$$G_s = \int_0^{4\pi} L_s(z, \theta) d\Omega, \quad \mathbf{q}_s = \int_0^{4\pi} L_s(z, \theta) \mathbf{s} d\Omega.$$

The \mathbf{q}_s has vanishing x and y components because $L_s^d(z, \theta)$ is independent of ϕ . Therefore, we can express \mathbf{q}_s as $\mathbf{q}_s = -q_s \hat{\mathbf{z}}$, where $q_s = |\mathbf{q}_s|$. The equation that governs L_s can be formulated as follows

$$\frac{dL_s}{dz} + \frac{\tau_H n_s L_s}{\nu} = \frac{\omega \tau_H n_s}{4\pi \nu} (G_s(z) - A_1 q_s \nu). \quad (23)$$

The equilibrium state intensity can be separated into two components: the collimated part denoted by L_s^c and the diffuse part caused by scattering denoted by L_s^d . The equation governing the collimated component L_s^c is

$$\frac{dL_s^c}{dz} + \frac{\tau_H n_s L_s^c}{\nu} = 0, \quad (24)$$

subject to the boundary conditions

$$L_s^c(1, \theta) = L_t \delta(s - s_0), \quad (\pi/2 \leq \theta \leq \pi), \quad (25)$$

After calculating the governing equation for L_s^c with boundary condition, we find L_s^c

$$L_s^c = L_t \exp\left(\int_z^1 \frac{\tau_H n_s(z')}{\nu} dz'\right) \delta(s - s_0), \quad (26)$$

and the diffused part is governed by

$$\frac{dL_s^d}{dz} + \frac{\tau_H n_s L_s^d}{\nu} = \frac{\omega \tau_H n_s}{4\pi \nu} (G_s(z) - A_1 q_s \nu), \quad (27)$$

subject to the boundary conditions

$$L_s^d(1, \theta) = \frac{L_D}{\pi}, \quad (\pi/2 \leq \theta \leq \pi), \quad (28a)$$

$$L_s^d(0, \theta) = 0, \quad (0 \leq \theta \leq \pi/2). \quad (28b)$$

In the basic state, the total intensity $G_s = G_s^c + G_s^d$ is written as

$$G_s = G_s^c + G_s^d = \int_0^{4\pi} [L_s^c(z, \theta) + L_s^d(z, \theta)] d\Omega = L_t \exp\left(\frac{-\int_z^1 \tau_H n_s(z') dz'}{\cos \theta_0}\right) + \int_0^\pi L_s^d(z, \theta) d\Omega, \quad (29)$$

Similarly, radiative heat flux in the basic state is defined as

$$\mathbf{q}_s = \mathbf{q}_s^c + \mathbf{q}_s^d = \int_0^{4\pi} (L_s^c(z, \theta) + L_s^d(z, \theta)) \mathbf{s} d\Omega = -L_t (\cos \theta_0) \exp\left(\frac{\int_z^1 -\tau_H n_s(z') dz'}{\cos \theta_0}\right) \hat{\mathbf{z}} + \int_0^{4\pi} L_s^d(z, \theta) \mathbf{s} d\Omega. \quad (30)$$

Now, define a new variable as

$$\tau = \int_z^1 \tau_H n_s(z') dz',$$

Eqs. (29) and (30) lead to two coupled Fredholm integral equations of the second kind as

$$G_s(\tau) = \frac{\omega}{2} \int_0^{\tau_H} G_s(\tau') E_1(|\tau - \tau'|) d\tau' + e^{-\tau/\cos \theta_0} + 2I_D E_2(\tau) + A_1 \text{sgn}(\tau - \tau') q_s(\tau') E_2(|\tau - \tau'|), \quad (31)$$

$$q_s(\tau) = \frac{\omega}{2} \int_0^{\tau_H} A_1 q_s(\tau') E_3(|\tau - \tau'|) d\tau' + (\cos \theta_0) e^{-\tau/\cos \theta_0} + 2I_D E_3(\tau) + \text{sgn}(\tau - \tau') G_s(\tau') E_2(|\tau - \tau'|), \quad (32)$$

where $E_n(x)$ is the exponential integral of order n and $\text{sgn}(x)$ is the signum function. This coupled FIEs are solved by using method of subtraction of singularity.

The mean swimming direction in the basic state becomes

$$\langle \mathbf{p}_s \rangle = -M_s \frac{\mathbf{q}_s}{q_s} = M_s \hat{\mathbf{z}},$$

where $M_s = M(G_s)$.

In the basic state, the cell concentration $n_s(z)$ satisfy the following equation

$$\frac{dn_s}{dz} - V_c M_s n_s = 0, \quad (33)$$

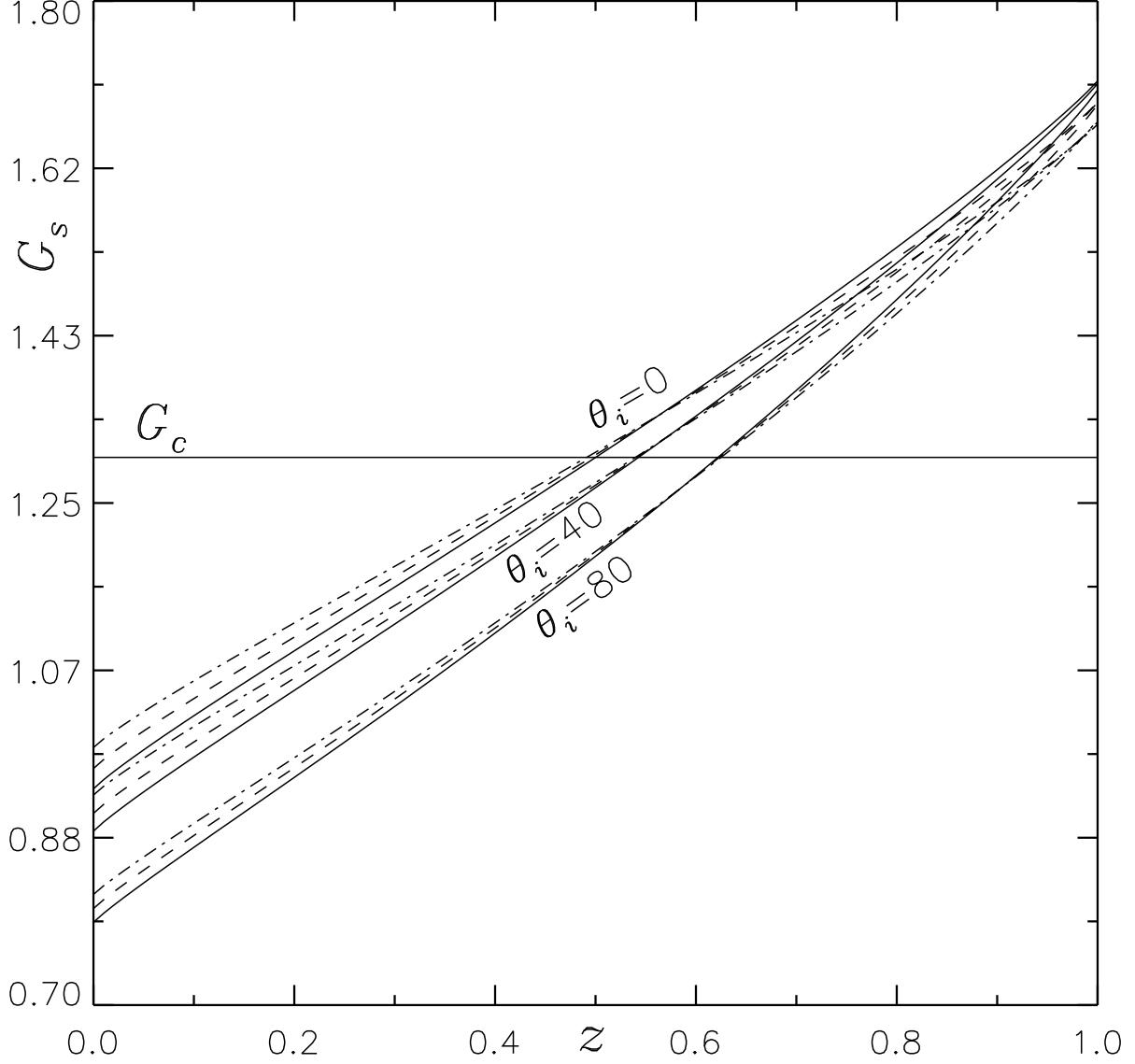


FIG. 3. Variation of total intensity in a uniform suspension by varying forward scattering coefficient A_1 from 0 to 0.8 for three different cases $\theta_i = 0, 40$ and 80 . Here, the governing parameter values $S_c = 20, V_c = 15, k = 0.5, \omega = 0.4$ and $L_t = 1$ are kept fixed.

which is supplemented by the equation

$$\int_0^1 n_s(z) dz = 1. \quad (34)$$

This equation shows the cell conservation relation. Eqs. (31) to (34) together form a boundary value problem, which can be solved through numerical techniques using the shooting method.

To illustrate the equilibrium solution, we keep $S_c = 20, G_c = 1.3, J_D = 0.26, \tau_H = 0.5, \omega = 0.4$, and $(\theta_i) = 0, 40, 80$ fixed. Then, we examine the forward scattering coefficient A_1 by varying A_1

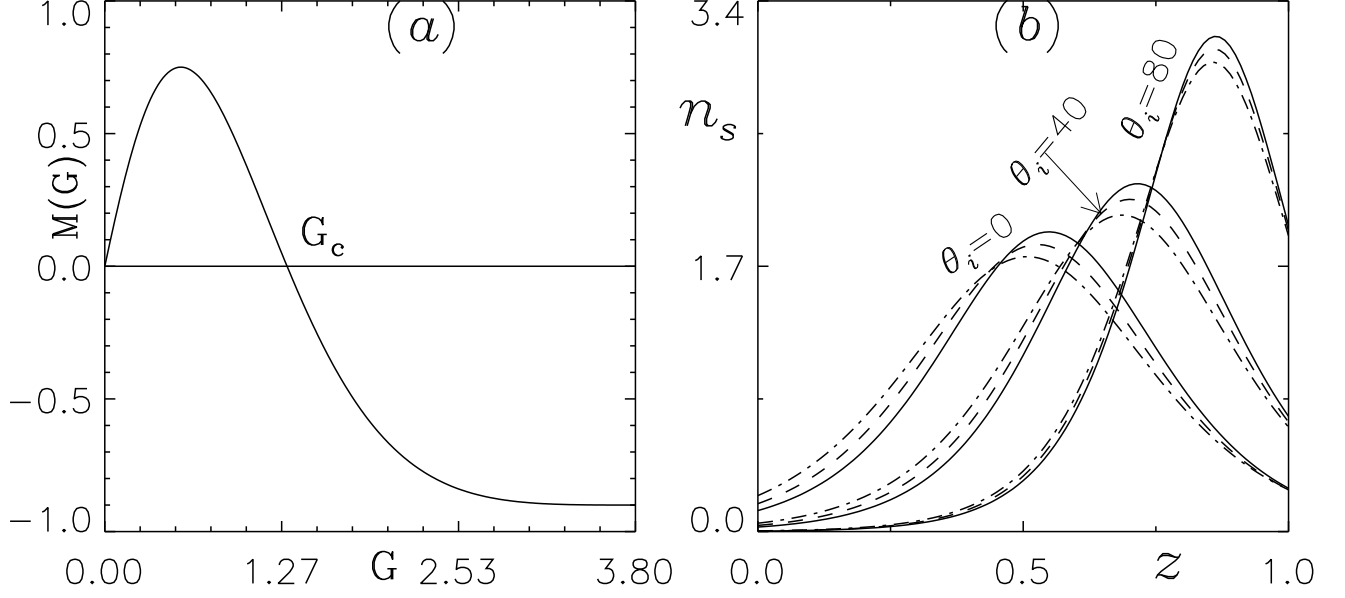


FIG. 4. (a) Taxis response curve for $G_c = 1.3$ and, (b) variation in base concentration profile by varying forward scattering coefficient A_1 from 0 to 0.8 for three different cases $\theta_i = 0, 40$ and 80 . Here, the governing parameter values $S_c = 20, V_c = 15, k = 0.5, \omega = 0.4$ and $I_i = 1$ are kept fixed.

from 0 to 0.8 on the total intensity and basic equilibrium solution.

Fig. 3 illustrates how the total intensity G_s varies with depth for a uniform suspension as the forward scattering coefficient A_1 is increased from 0 to 0.8. As A_1 increases, the height of the total intensity G_s at the lower half of the uniform suspension increases, while at the upper half, it decreases.

Fig. 4(a) displays a curve of phototaxis function for light intensity where $G_c = 1.3$ is the critical value. On the other hand, Fig. 4(b) presents the influence of the forward scattering coefficient A_1 on the sublayer at equilibrium state for the same governing parameters. When $\theta_i = 0$, the sublayer forms at mid-height of the suspension domain under equilibrium state. When A_1 is raised from 0 to 0.8, the sublayer location at equilibrium state shifts towards the bottom. Similarly, for $\theta_i = 40$ and 80 , the sublayer at equilibrium state is located around three-quarter height and top of the suspension depth, respectively. Increasing A_1 from 0 to 0.8 causes the sublayer at equilibrium state to shift towards the bottom in each case.

IV. LINEAR STABILITY OF THE PROBLEM

To analyze stability, linear perturbation theory is employed, which involves introducing a small perturbation of amplitude $\varepsilon \ll 1$ to the equilibrium state using the following equation

$$\begin{aligned} [\mathbf{U}, n, L, \langle \mathbf{p} \rangle] &= [0, n_s, L_s, \langle \mathbf{p}_s \rangle] + \varepsilon [\mathbf{U}_1, n_1, L_1, \langle \mathbf{p}_1 \rangle] + \mathcal{O}(\varepsilon^2) \\ &= [0, n_s, L_s^c + L_s^d, \langle \mathbf{p}_s \rangle] + \varepsilon [\mathbf{U}_1, n_1, L_1^c + L_1^d, \langle \mathbf{p}_1 \rangle] + \mathcal{O}(\varepsilon^2). \end{aligned} \quad (35)$$

The perturbed variables are inserted into equations (12) to (14), and linearization is performed by collecting terms of $o(\varepsilon)$ terms about the equilibrium state, which yields

$$\nabla \cdot \mathbf{U}_1 = 0, \quad (36)$$

where $\mathbf{U}_1 = (U_1, V_1, W_1)$.

$$S_c^{-1} \left(\frac{\partial \mathbf{U}_1}{\partial t} \right) + \nabla P_e + R n_1 \hat{\mathbf{z}} = \nabla^2 \mathbf{U}_1, \quad (37)$$

$$\frac{\partial n_1}{\partial t} + V_c \nabla \cdot (\langle \mathbf{p}_s \rangle n_1 + \langle \mathbf{p}_1 \rangle n_s) + W_1 \frac{dn_s}{dz} = \nabla^2 n_1. \quad (38)$$

If $G = G_s + \varepsilon G_1 + \mathcal{O}(\varepsilon^2) = (G_s^c + \varepsilon G_1^c) + (G_s^d + \varepsilon G_1^d) + \mathcal{O}(\varepsilon^2)$, then the steady collimated total intensity is perturbed and after simplification, we get

$$G_1^c = L_t \exp \left(\frac{-\int_z^1 \tau_H n_s(z') dz'}{\cos \theta_0} \right) \left(\frac{\int_1^z \tau_H n_1 dz'}{\cos \theta_0} \right) \quad (39)$$

and, G_1^d is given by

$$G_1^d = \int_0^{4\pi} L_1^d(\mathbf{x}, \mathbf{s}) d\Omega. \quad (40)$$

In the similar manner, we can find perturbed radiative heat flux as

$$\mathbf{q}_1^c = -I_t(\cos \theta_0) \exp \left(\frac{-\int_z^1 \tau_H n_s(z') dz'}{\cos \theta_0} \right) \left(\frac{\int_1^z \tau_H n_1 dz'}{\cos \theta_0} \right) \hat{\mathbf{z}} \quad (41)$$

and

$$\mathbf{q}_1^d = \int_0^{4\pi} L_1^d(\mathbf{x}, \mathbf{s}) \mathbf{s} d\Omega. \quad (42)$$

Now the expression

$$-M(G_s + \varepsilon G_1) \frac{\mathbf{q}_s + \varepsilon \mathbf{q}_1 + \mathcal{O}(\varepsilon^2)}{|\mathbf{q}_s + \varepsilon \mathbf{q}_1 + \mathcal{O}(\varepsilon^2)|} - M_s \hat{\mathbf{z}},$$

gives the perturbed swimming direction on collecting $O(\varepsilon)$ terms

$$\langle \mathbf{p}_1 \rangle = G_1 \frac{dM_s}{dG} \hat{z} - M_s \frac{\mathbf{q}_1^H}{q_s}, \quad (43)$$

where $\mathbf{q}_1^H = [q_1^x, q_1^y]$ is the horizontal component of the perturbed radiative flux \mathbf{q}_1 . Now substituting the value of $\langle \mathbf{p}_1 \rangle$ from Eq. (46) into Eq. (41) and simplifying, we get

$$\frac{\partial n_1}{\partial t} + V_c \frac{\partial}{\partial z} \left(M_s n_1 + n_s G_1 \frac{dM_s}{dG} \right) - V_c n_s \frac{M_s}{q_s} \left(\frac{\partial q_1^x}{\partial x} + \frac{\partial q_1^y}{\partial y} \right) + W_1 \frac{dn_s}{dz} = \nabla^2 n_1. \quad (44)$$

By taking the double curl and z-component of Eq.(37), we can eliminate the pressure gradient P_e and the horizontal component of u_1 . This results in a reduction of Eqs.(37), (38), and (44) to two equations for W_1 and n_1 , which can be decomposed into normal modes as

$$W_1 = \tilde{W}(z) \exp(\gamma t + i(lx + my)), \quad n_1 = \tilde{N}(z) \exp(\gamma t + i(lx + my)). \quad (45)$$

The governing equation for perturbed intensity L_1 can be written as

$$\xi \frac{\partial L_1}{\partial x} + \eta \frac{\partial L_1}{\partial y} + \nu \frac{\partial L_1}{\partial z} + \tau_H (n_s L_1 + n_1 L_s) = \frac{\omega \tau_H}{4\pi} (n_s G_1 + G_s n_1 + A_1 \mathbf{v} \cdot (n_s \mathbf{q}_1 - q_s n_1)), \quad (46)$$

subject to the boundary conditions

$$L_1(x, y, z = 1, \xi, \eta, \nu) = 0, \quad (\pi/2 \leq \theta \leq \pi, 0 \leq \phi \leq 2\pi), \quad (47a)$$

$$L_1(x, y, z = 0, \xi, \eta, \nu) = 0, \quad (0 \leq \theta \leq \pi/2, 0 \leq \phi \leq 2\pi). \quad (47b)$$

The Eq. (46) indicates that L_1^d can be expressed as follows

$$L_1^d = \Psi^d(z, \xi, \eta, \nu) \exp(\gamma t + i(lx + my)).$$

From Eqs. (39) and (40), we get

$$G_1^c = \left[L_r \exp \left(\frac{-\int_z^1 \tau_H n_s(z') dz'}{\cos \theta_0} \right) \left(\frac{\int_1^z \tau_H n_1 dz'}{\cos \theta_0} \right) \right] \exp(\gamma t + i(lx + my)) = \mathbb{G}^c(z) \exp(\gamma t + i(lx + my)), \quad (48)$$

and

$$G_1^d = \mathbb{G}^d(z) \exp(\gamma t + i(lx + my)) = \left(\int_0^{4\pi} \Psi^d(z, \xi, \eta, \nu) d\Omega \right) \exp(\gamma t + i(lx + my)), \quad (49)$$

where $\mathbb{G}(z) = \mathbb{G}^c(z) + \mathbb{G}^d(z)$ is the perturbed total intensity. Similarly from Eqs. (41) and (42), we have

$$\mathbf{q}_1 = [q_1^x, q_1^y, q_1^z] = [P(z), Q(z), S(z)] \exp[\gamma t + i(lx + my)],$$

where

$$[P(z), Q(z)] = \int_0^{4\pi} [\xi, \eta] \Psi^d(z, \xi, \eta, \nu) d\Omega,$$

Note that the $P(z)$ and $Q(z)$ appears due to scattering. On the other hand $S(z)$ has both collimated and diffuse part. The collimated part of $S(z)$ is same as q_1^c . Therefore, $S(z)$ is given by

$$S(z) = q_1^c + \int_0^{4\pi} \Psi^d(z, \xi, \eta, \nu) \nu d\Omega,$$

Now, Ψ^d satisfies

$$\frac{d\Psi^d}{dz} + \frac{(i(l\xi + m\eta) + \tau_H n_s)}{\nu} \Psi^d = \frac{\omega \tau_H}{4\pi \nu} (n_s \mathbb{G} + G_s \tilde{N}(z) + A_1 \nu (n_s S - q_s \tilde{N}(z))) - \frac{\tau_H}{\nu} I_s \tilde{N}(z), \quad (50)$$

subject to the boundary conditions

$$\Psi^d(1, \xi, \eta, \nu) = 0, \quad (\pi/2 \leq \theta \leq \pi, 0 \leq \phi \leq 2\pi), \quad (51a)$$

$$\Psi^d(0, \xi, \eta, \nu) = 0, \quad (0 \leq \theta \leq \pi/2, 0 \leq \phi \leq 2\pi). \quad (51b)$$

The linear stability equations become

$$\left(\gamma S_c^{-1} + k^2 - \frac{d^2}{dz^2} \right) \left(\frac{d^2}{dz^2} - k^2 \right) \tilde{W} = R k^2 \tilde{N}(z), \quad (52)$$

$$\left(\gamma + k^2 - \frac{d^2}{dz^2} \right) \tilde{N}(z) + V_c \frac{d}{dz} \left(M_s \tilde{N}(z) + n_s \mathbb{G} \frac{dM_s}{dG} \right) - i \frac{V_c n_s M_s}{q_s} (lP + mQ) = - \frac{dn_s}{dz} \tilde{W}(z), \quad (53)$$

subject to the boundary conditions

$$\tilde{W}(z) = \frac{d\tilde{W}(z)}{dz} = \frac{d\tilde{N}(z)}{dz} - V_c M_s \tilde{N}(z) - n_s V_c \mathbb{G} \frac{dM_s}{dG} = 0, \quad \text{at } z = 0, 1. \quad (54)$$

Here k represents the non-dimensional wavenumber, which is determined by the square root of the sum of the squares of l and m . Eqs. (52)-(53) constitute an eigenvalue problem that describes γ as a function of various dimensionless parameters, including V_c , τ_H , ω , J_D , θ_i , A_1 , l , m , and R . Equation (53) can be expressed as

$$\Lambda_0(z) + \Lambda_1(z) \int_1^z \tilde{N}(z) dz + (\gamma + k^2 + \Lambda_2(z)) \tilde{N}(z) + \Lambda_3(z) D \tilde{N}(z) - D^2 \tilde{N}(z) = -D n_s \tilde{W}, \quad (55)$$

where

$$\Lambda_0(z) = V_c D \left(n_s \mathbb{G} \frac{dM_s}{dG} \right) - i \frac{V_c n_s M_s}{q_s} (lP + mQ), \quad (56a)$$

$$\Lambda_1(z) = \tau_H V_c D \left(n_s G_s^c \frac{dM_s}{dG} \right) \quad (56b)$$

$$\Lambda_2(z) = 2\tau_H V_c n_s G_s^c \frac{dM_s}{dG} + V_c \frac{dM_s}{dM} D G_s^d, \quad (56c)$$

$$\Lambda_3(z) = V_c M_s. \quad (56d)$$

Introducing the new variable

$$\tilde{\Theta}(z) = \int_1^z \tilde{N}(z') dz', \quad (57)$$

the linear stability equations become

$$(\gamma S_c^{-1} + k^2 - D^2) (D^2 - k^2) \tilde{W} = R k^2 D \tilde{\Theta}, \quad (58)$$

$$\Lambda_0(z) + \Lambda_1(z) \tilde{\Theta} + (\gamma + k^2 + \Lambda_2(z)) D \tilde{\Theta} + \Lambda_3(z) D^2 \tilde{\Theta} - D^3 \tilde{\Theta} = -D n_s \tilde{W}. \quad (59)$$

The boundary conditions become,

$$\tilde{W} = D \tilde{W} = D^2 \tilde{\Theta} - \Lambda_2(z) D \tilde{\Theta} - \Lambda_3(z) \frac{dM_s}{dG} \mathbb{G} = 0, \quad \text{at } z = 0, 1, \quad (60)$$

and the additional boundary condition is

$$\tilde{\Theta}(z) = 0, \quad \text{at } z = 1. \quad (61)$$

V. SOLUTION PROCEDURE

To solve Eqs. (58) and (59) and calculate the neutral (marginal) stability curves or the growth rate, $Re(\gamma)$, as a function of R in the (k, R) -plane for a fixed set of other parameters, a fourth-order accurate, finite-difference scheme based on Newton-Raphson-Kantorovich (NRK) iterations²³ is utilized. The graph of points for which $Re(\gamma) = 0$ is called a marginal (neutral) stability curve. If the condition $Im(\gamma) = 0$ is satisfied on such a curve, then the bioconvective solution is called stationary (non-oscillatory), and oscillatory solutions exist if $Im(\gamma) \neq 0$. Overstability occurs if the most unstable mode remains on the oscillatory branch of the neutral curve. When an oscillatory solution occurs, a common point (k_b) exists between the stationary and oscillatory branches, and in this instance, the oscillatory branch is the locus of points for which $k \leq k_b$. A particular most unstable mode, i.e. (k_c, R_c) , of the neutral curve $R^{(n)}(k)$ ($n = 1, 2, 3, \dots$) is selected, and in this instance, the wavelength of the initial disturbance is calculated as $\lambda_c = 2\pi/k_c$. A bioconvective solution is called mode n if n convection cells can be organized such that one overlies another vertically¹⁸. Additionally, the estimated parameters for the proposed problem are the same as previous studies^{12,13,17,18,20}.

VI. NUMERICAL RESULTS

We use a discrete set of fixed parameters to determine the most unstable mode from an initial equilibrium solution. These parameters include $S_c = 20$, $G_c = 1.3$, $V_c = 10, 15, 20$, $\omega = 0.4$, $J_D = 0.26, 0.48$, $\theta_i = 0, 40, 80$, and $\tau_H = 0.5, 1$, while varying A_1 as $A_1 = 0, 0.4, 0.8$. To investigate the influence of forward scattering on bioconvection, we consider discrete values of the angle of incidence ($\theta_i = 0, 40, 80$). For $\theta_i = 0$, the sublayer location at equilibrium state is approximately at mid-height of the domain. As θ_i increases to 40 and 80, the sublayer location is shift from mid-height to three-quarter height, and top of the domain, respectively. The width of the unstable region (WUR) refers to the distance from the equilibrium state sublayer location to the bottom of the domain, while the concentration difference in the unstable region (CDUR) is defined as the difference between the maximum concentration and the concentration at the bottom of the suspension. If the WUR or CDUR is higher, it indicates that the suspension is more unstable.

A. WHEN FORWARD SCATTERING IS WEAKER THAN SELF-SHADING

The effect of forward scattering on the onset of bioconvection is studied by considering the effectiveness of self-shading compared to scattering, which is achieved by selecting a lower value of the scattering albedo ω . Additionally, the strength of self-shading is varied by selecting different values of the extinction coefficient τ_H , specifically, a high value of $\tau_H = 1$ indicates strong self-shading, while a low value of $\tau_H = 0.5$ indicates weak self-shading. Throughout the study, a critical intensity of $g_c = 1.3$ is used.

I. $V_c = 15$

(i) When extinction coefficient $\tau_H = 0.5$

In this section, the effects of the forward scattering coefficient A_1 on bioconvective instability at angle of incidence $\theta_i = 0, 40, 80$ are discussed for a set of fixed parameters $V_c = 15$, $\tau_H = 0.5$, $\omega = 0.4$ and $J_D = 0.26$. We vary the value of A_1 from 0 to 0.8 and study the resulting changes in the sublayer location at equilibrium state, as well as WUR and CDUR.

When $\theta_i = 0$, sublayer occurs at the mid-height of the domain for $A_1 = 0$. As A_1 increases, the sublayer at equilibrium state shifts towards the bottom of the domain, resulting in a decrease in both the WUR and CDUR. Consequently, the critical Rayleigh number, which is a measure of the

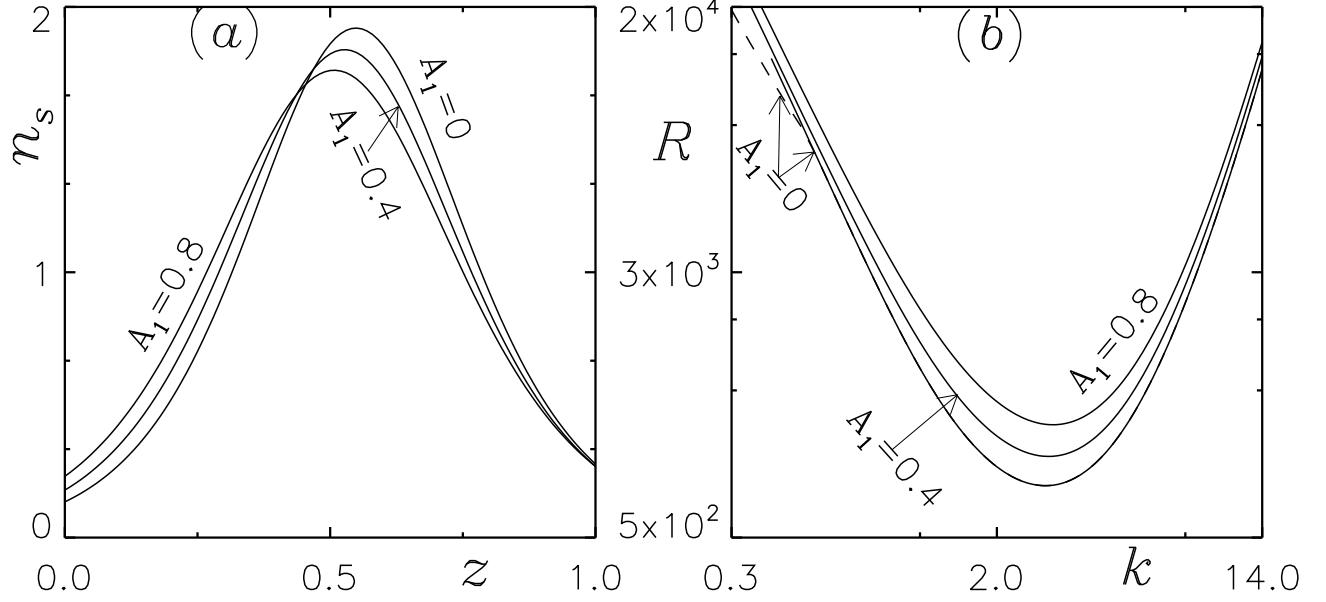


FIG. 5. (a) Basic concentration profile, (b) corresponding marginal stability curves for different values of angle of incidence θ_i . Here, the governing parameter values $S_c = 20, V_c = 15, k = 0.5, I_D = 0.26$, and $\omega = 0.4$ are kept fixed.

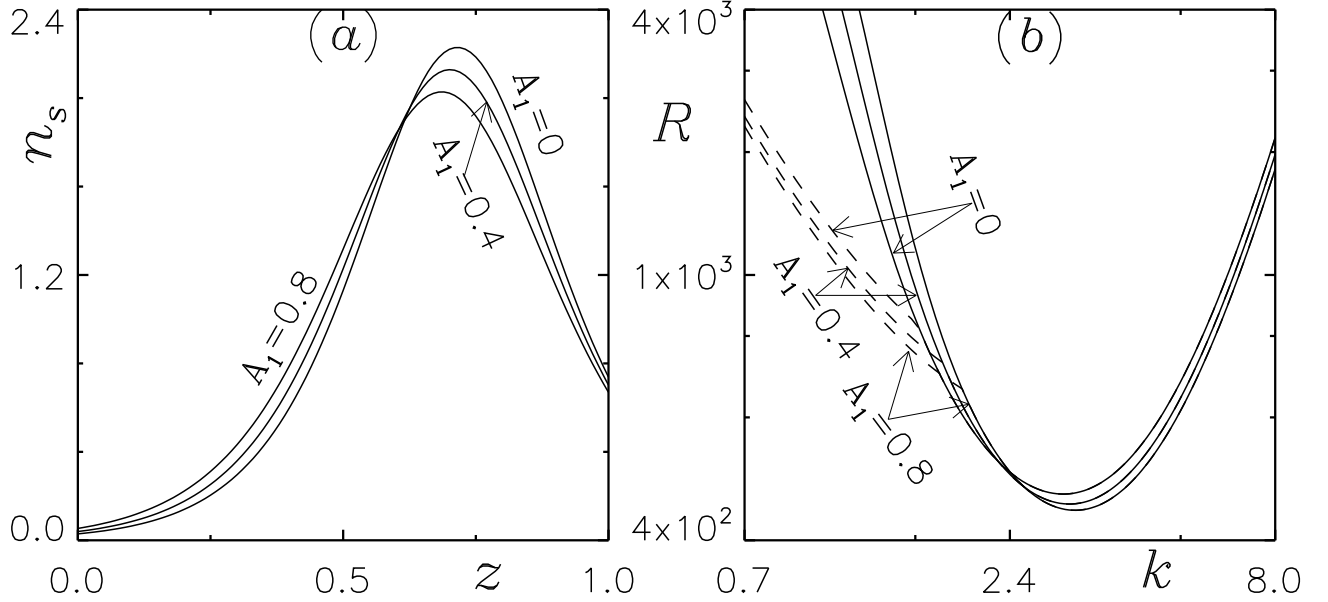


FIG. 6. (a) Basic concentration profile, (b) corresponding marginal stability curves for different values of angle of incidence θ_i . Here, the governing parameter values $S_c = 20, V_c = 15, k = 0.5, I_D = 0.26$, and $\omega = 0.4$ are kept fixed.

suspension's stability, increases as A_1 is increased from 0 to 0.8. As a result, suspension stability

increases (see Fig. 5).

For $\theta_i = 40$, the location of the sublayer is at three-quarter height of the domain when $A_1 = 0$. The location of the sublayer shift towards the midheight of the domain, as A_1 increases to 0.4 and 0.8. In this case, WUR and CDUR both decreases as A_1 increases. As a result, the critical Rayleigh number increases and suspension becomes more stable similar to the case of $\theta_i = 0$ (see Fig. 6).

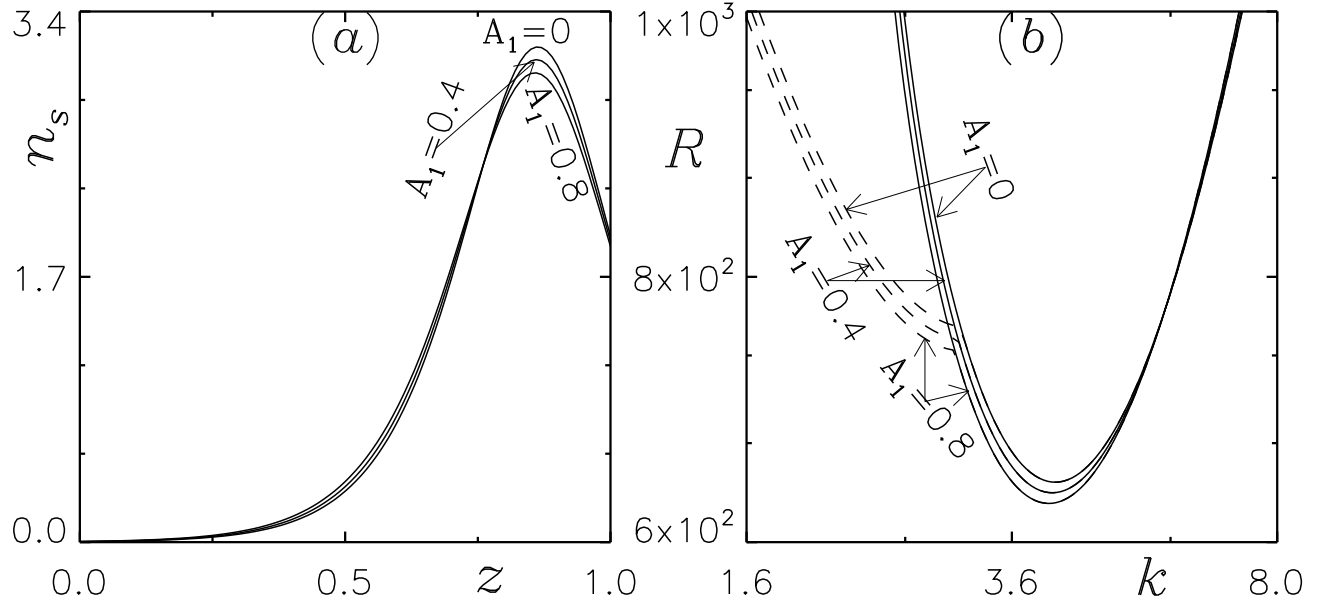


FIG. 7. (a) Basic concentration profile, (b) corresponding marginal stability curves for different values of angle of incidence θ_i . Here, the governing parameter values $S_c = 20, V_c = 15, k = 0.5, I_D = 0.26$, and $\omega = 0.4$ are kept fixed.

For $\theta_i = 80$, sublayer forms nearer to the top of the domain. Here, WUR remains same for all cases $A_1 = 0, 0.4$, and 0.8 , but CDUR decreases as A_1 is increased from 0 to 0.8. In this instance, the decrease in CDUR is more dominant than the change in WUR, resulting in a decrease in critical Rayleigh number and making the suspension less stable (see Fig. 7).

One more interesting phenomenon (bifurcation of oscillatory branch from the stationary branch) of the solution is also observed here. This is observed when $\theta_i = 0$ for $A_1 = 0$ and when $\theta_i = 40, 80$ for all values of A_1 , but most unstable mode from an initial equilibrium solution is stationary for all values of θ_i .

(ii) When extinction coefficient $\tau_H = 1$

Let's examine the effect of forward scattering effect where $V_c = 15, \tau_H = 1, \omega = 0.4$, and $J_D = 0.48$

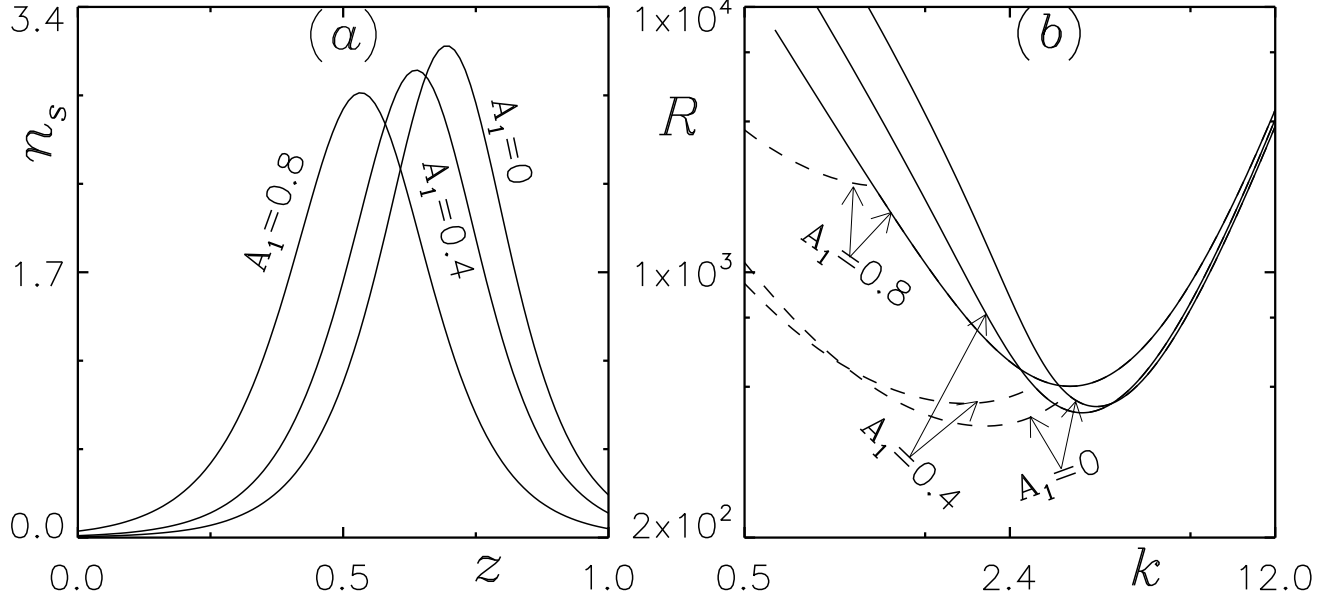


FIG. 8. (a) Basic concentration profile, (b) corresponding marginal stability curves for different values of angle of incidence θ_i . Here, the governing parameter values $S_c = 20, V_c = 15, k = 0.5, I_D = 0.26$, and $\omega = 0.4$ are kept fixed.

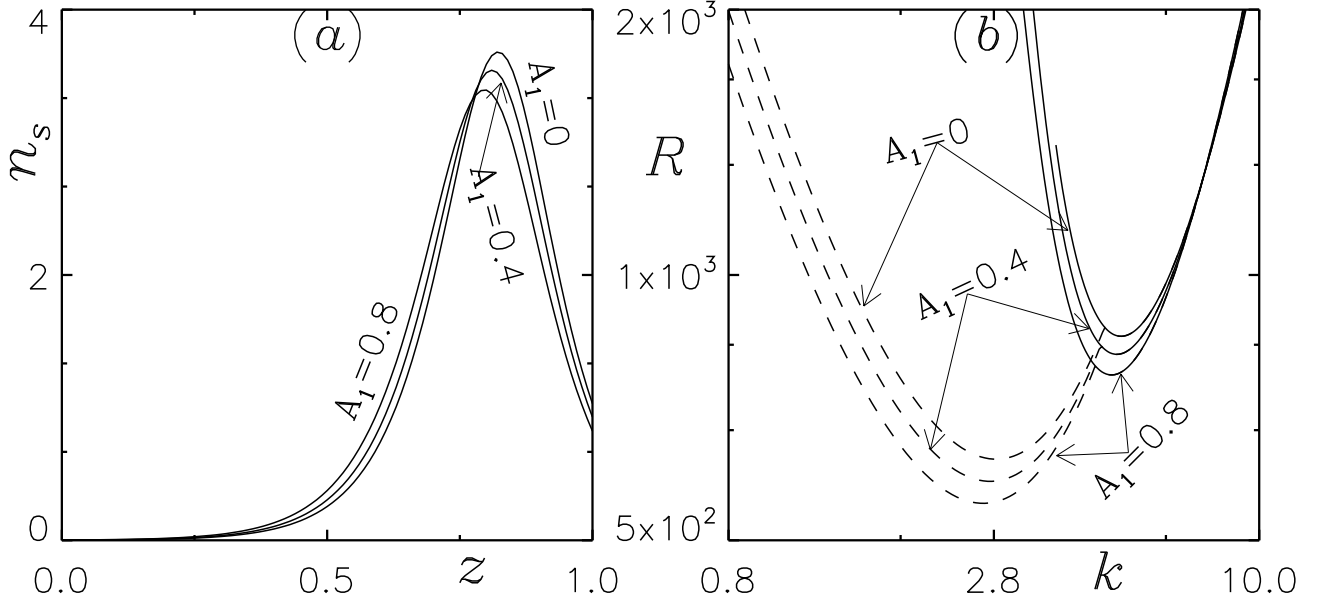


FIG. 9. (a) Basic concentration profile, (b) corresponding marginal stability curves for different values of angle of incidence θ_i . Here, the governing parameter values $S_c = 20, V_c = 15, k = 0.5, I_D = 0.26$, and $\omega = 0.4$ are kept fixed.

at $\theta_i = 0, 40$, and 80 .

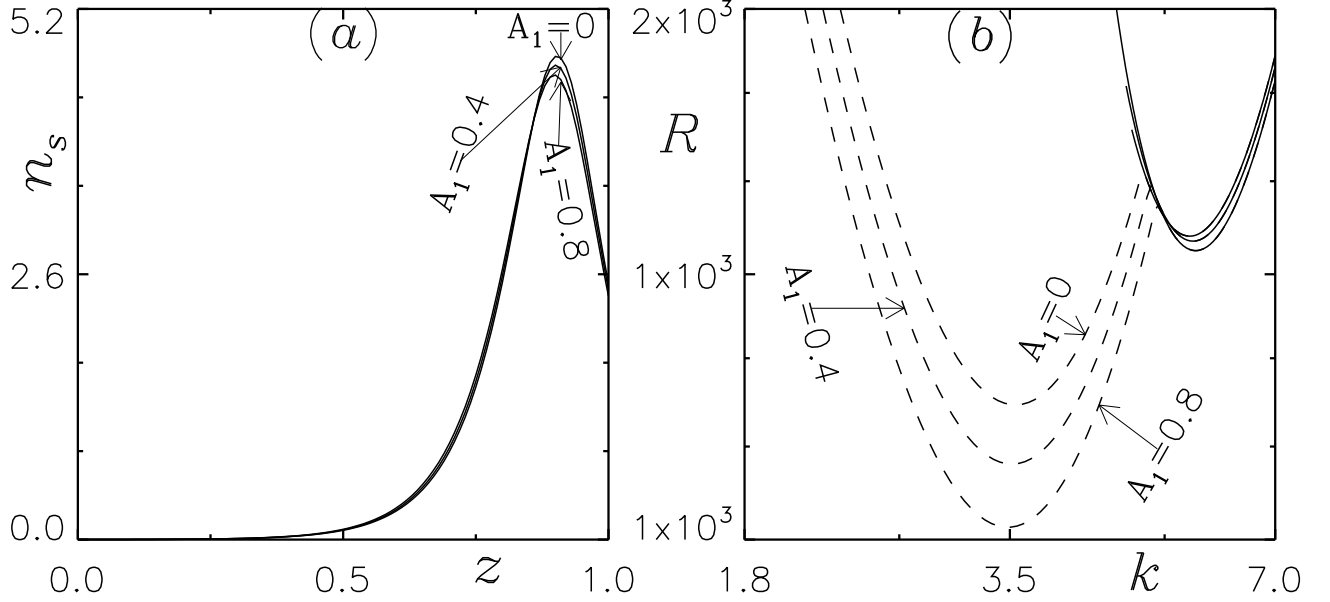


FIG. 10. (a) Basic concentration profile, (b) corresponding marginal stability curves for different values of angle of incidence θ_i . Here, the governing parameter values $S_c = 20, V_c = 15, k = 0.5, I_D = 0.26$, and $\omega = 0.4$ are kept fixed.

For the case when $\theta_i = 0$, the sublayer at equilibrium state forms approximately at a mid-height of the domain, and as A_1 increases to 0.4 and 0.8, the location of the sublayer shifts towards the bottom of the domain. Here, WUR and CDUR both decreases as A_1 is increased. As a result, critical Rayleigh number is increased and suspension becomes more stable. In this case, an oscillatory branch bifurcate from the stationary branch of the marginal stability curve but only for $A_1 = 0$, the solution becomes overstable (see Fig. 8).

Now, for $\theta_i = 40$, When $A_1 = 0$, the sublayer at equilibrium state forms approximately at around three-quarter height of the domain, and the location of the sublayer at equilibrium state shifts towards the mid-height as A_1 increases to 0.4 and 0.8. Here, in WUR a very small decrement is observed with increment in A_1 , but CDUR decreases considerably as A_1 is increased from 0 to 0.8. In this instance, the decrease in CDUR is more effective than the decrease in WUR, resulting in a decrease in critical Rayleigh number and making the suspension less stable. Here, the most unstable mode in the initial equilibrium solution is overstable for all value of A_1 .

Finally, for $\theta_i = 80$, the sublayer equilibrium state forms at approximately at the $z = 0.9$ of the domain, and the location of the sublayer at equilibrium state shifts towards the three-quarter height of the domain as A_1 increases to 0.4 and 0.8. Due to the same region to the case of $\theta_i = 40$, the

critical Rayleigh number decrease as A_1 is increased. Here, oscillatory branch bifurcates from the stationary branch in all three cases and the most unstable mode in the initial equilibrium solution is overstable. Table I summarizes the numerical results for the critical Rayleigh number (R_c) and the wavelength (λ_c) of this section.

TABLE I. The quantitative values of bioconvective solutions with increment in I_D for $V_c = 15$ are shown in the table, where other parameters are kept fixed.

V_c	τ_H	ω	L_D	θ_i	A_1	λ_c	R_c	$Im(\gamma)$
15	0.5	0.4	0.26	0	0 ^a	2	718.98	0
15	0.5	0.4	0.26	0	0.4	2	882.36	0
15	0.5	0.4	0.26	0	0.8	1.96	1101.18	0
15	0.5	0.4	0.26	40	0 ^a	1.53	452.20	0
15	0.5	0.4	0.26	40	0.4 ^a	1.57	463.92	0
15	0.5	0.4	0.26	40	0.8 ^a	1.62	483.92	0
15	0.5	0.4	0.26	80	0 ^a	1.2	648.90	0
15	0.5	0.4	0.26	80	0.4 ^a	1.8	640.01	0
15	0.5	0.4	0.26	80	0.8 ^a	1.8	631.11	0
15	1	0.4	0.48	0	0	2.96 ^b	459.78 ^b	12.58
15	1	0.4	0.48	0	0.4 ^a	1.67	507.67	0
15	1	0.4	0.48	0	0.8 ^a	1.79	618.54	0
15	1	0.4	0.48	40	0	2.18 ^b	618.01 ^b	20.06
15	1	0.4	0.48	40	0.4	2.24 ^b	583.28 ^b	19.22
15	1	0.4	0.48	40	0.8	2.32 ^b	550.74 ^b	18.19
15	1	0.4	0.48	80	0	1.74 ^b	1190.06 ^b	21.01
15	1	0.4	0.48	80	0.4	1.76 ^b	1149.62 ^b	21.89
15	1	0.4	0.48	80	0.8	1.77 ^b	1108.00 ^b	22.53

^a A result indicates that the $R^{(1)}(k)$ branch of the neutral curve is oscillatory.

^b A result indicates that a smaller solution occurs on the oscillatory branch.

2. $V_c = 10$ and $V_c = 20$

The results of the numerical analysis for the bioconvective instability at different values of the forward scattering coefficient for $V_c = 10$ and 20 show a similar trend to that observed for $V_c = 15$ in terms of the behavior of the most unstable mode from an equilibrium solution. The details of the numerical results for bioconvective instability are presented in Table II and Table III.

TABLE II. The quantitative values of bioconvective solutions with increment in I_D for $V_c = 15$ are shown in the table, where other parameters are kept fixed.

V_c	τ_H	ω	L_D	θ_i	A_1	λ_c	R_c	$Im(\gamma)$
10	0.5	0.4	0.26	0	0	2.24	1335.27	0
10	0.5	0.4	0.26	0	0.4	2.2	1577.07	0
10	0.5	0.4	0.26	0	0.8	2.11	1884.13	0
10	0.5	0.4	0.26	40	0	2.61	619.83	0
10	0.5	0.4	0.26	40	0.4	2.61	676.10	0
10	0.5	0.4	0.26	40	0.8	2.61	745.77	0
10	0.5	0.4	0.26	80	0 ^a	2.15	457.32	0
10	0.5	0.4	0.26	80	0.4 ^a	2.2	460.12	0
10	0.5	0.4	0.26	80	0.8	2.24	463.82	0
10	1	0.4	0.48	0	0 ^a	1.96	592.73	0
10	1	0.4	0.48	0	0.4 ^a	2	700.48	0
10	1	0.4	0.48	0	0.8	1.96	886.08	0
10	1	0.4	0.48	40	0 ^a	1.69	533.12	0
10	1	0.4	0.48	40	0.4 ^a	1.72	531.64	0
10	1	0.4	0.48	40	0.8 ^a	1.75	534.64	0
10	1	0.4	0.48	80	0 ^a	1.53	695.41	0
10	1	0.4	0.48	80	0.4 ^a	1.53	692.53	0
10	1	0.4	0.48	80	0.8	1.53	688.86	0

^a A result indicates that the $R^{(1)}(k)$ branch of the neutral curve is oscillatory.

^b A result indicates that a smaller solution occurs on the oscillatory branch.

TABLE III. The quantitative values of bioconvective solutions with increment in I_D for $V_c = 15$ are shown in the table, where other parameters are kept fixed.

V_c	τ_H	ω	L_D	θ_i	A_1	λ_c	R_c	$Im(\gamma)$
20	0.5	0.4	0.26	0	0 ^a	2	478.48	0
20	0.5	0.4	0.26	0	0.4 ^a	2	577.36	0
20	0.5	0.4	0.26	0	0.8 ^a	1.96	753.15	0
20	0.5	0.4	0.26	40	0 ^a	1.53	552.23	0
20	0.5	0.4	0.26	40	0.4 ^a	1.57	536.7	0
20	0.5	0.4	0.26	40	0.8 ^a	1.62	524.43	0
20	0.5	0.4	0.26	80	0 ^a	1.2	1049.65	0
20	0.5	0.4	0.26	80	0.4	1.8 ^b	1017 ^b	16.06
20	0.5	0.4	0.26	80	0.8	1.8 ^b	984.16 ^b	15.63
20	1	0.4	0.48	0	0	2.67 ^b	423.32 ^b	21.58
20	1	0.4	0.48	0	0.4	3.04 ^b	379.34 ^b	17.56
20	1	0.4	0.48	0	0.8	2.72 ^b	718.49 ^b	12.04
20	1	0.4	0.48	40	0	1.93 ^b	820.65 ^b	35.14
20	1	0.4	0.48	40	0.4	1.96 ^b	750.14 ^b	33.71
20	1	0.4	0.48	40	0.8	2.05 ^b	680.13 ^b	31.83
20	1	0.4	0.48	80	0	1.49 ^b	1854.42 ^b	38.81
20	1	0.4	0.48	80	0.4	1.52 ^b	1779.89 ^b	40.09
20	1	0.4	0.48	80	0.8	1.52 ^b	1702.46 ^b	40.98

^a A result indicates that the $R^{(1)}(k)$ branch of the neutral curve is oscillatory.

^b A result indicates that a smaller solution occurs on the oscillatory branch.

VII. CONCLUSION

The proposed phototaxis model investigates the impact of rigid top surface on the onset of light induced bioconvection in an anisotropic (forward) scattering algal suspension illuminated by both diffuse and oblique (not vertical) collimated flux. A linear anisotropic scattering coefficient is used in this analysis. An initial equilibrium solution at the bioconvective instability is also investigated by using the linear analysis of the same suspension.

When the forward scattering coefficient A_1 is increased in a uniform suspension, the total intensity decreases in the upper half and increases in the lower half of the suspension at the equilibrium state. Furthermore, the critical value of total intensity decrease (increase) in the lower (upper) half of the suspension as A_1 is increased. As A_1 is increased, the sublayer position shift towards the bottom of the domain. On the other hand, concentration in the sublayer also increases as the A_1 is increased.

When the sublayer at equilibrium state forms near the mid-height of the domain, the critical wavelength decreases and critical Rayleigh number increases with an increase in the forward scattering coefficient A_1 . When sublayer forms nearer to the top of the domain, as A_1 is increased, the critical Rayleigh number and critical wavelength both decreases. On the other hand, when sublayer occurs around at three-quarter height of the domain, the critical rayleigh number and critical wavelength both increases for weak self-shading suspension but for strong self-shading suspension, the critical wavelength increases and critical Rayleigh number decreases as A_1 is increased.

It seems that the behavior of the bioconvective solutions depends on the self-shading effect in the suspension. For weak self-shading suspension, an oscillatory branch bifurcate from the stationary branch of the marginal stability curve but most unstable solution occurs on the stationary branch. Therefore, almost every position of the sulayer solution remains stationary. But, for strong self-shading suspension, the bio-convective solution convert into overstable solution for almost all locations for the sublayer at equilibrium state.

ACKNOWLEDGMENTS

The author gratefully acknowledges the Ministry of Education (Government of India) for the financial support via GATE fellowship (Registration No. MA19S43047204).

DATA AVAILABILITY

The data that support the plots within this paper and other findings of this study are available within the article.

REFERENCES

- ¹J. R. Platt, ““ bioconvection patterns” in cultures of free-swimming organisms,” *Science* **133**, 1766–1767 (1961).
- ²T. J. Pedley and J. O. Kessler, “Hydrodynamic phenomena in suspensions of swimming microorganisms,” *Annual Review of Fluid Mechanics* **24**, 313–358 (1992).
- ³N. A. Hill and T. J. Pedley, “Bioconvection,” *Fluid Dynamics Research* **37**, 1 (2005).
- ⁴M. A. Bees, “Advances in bioconvection,” *Annual Review of Fluid Mechanics* **52**, 449–476 (2020).
- ⁵A. Javadi, J. Arrieta, I. Tuval, and M. Polin, “Photo-bioconvection: towards light control of flows in active suspensions,” *Philosophical Transactions of the Royal Society A* **378**, 20190523 (2020).
- ⁶H. Wager, “VII. on the effect of gravity upon the movements and aggregation of euglena viridis, ehrb., and other micro-organisms,” *Philosophical Transactions of the Royal Society of London. Series B, Containing Papers of a Biological Character* **201**, 333–390 (1911).
- ⁷J. O. Kessler, “Co-operative and concentrative phenomena of swimming micro-organisms,” *Contemporary Physics* **26**, 147–166 (1985).
- ⁸J. O. Kessler and N. A. Hill, “Complementarity of physics, biology and geometry in the dynamics of swimming micro-organisms,” in *Physics of biological systems* (Springer, 1997) pp. 325–340.
- ⁹J. O. Kessler, “The external dynamics of swimming micro-organisms,” *Progress in phycological research* **4**, 258–307 (1986).
- ¹⁰C. R. Williams and M. A. Bees, “A tale of three taxes: photo-gyro-gravitactic bioconvection,” *Journal of Experimental Biology* **214**, 2398–2408 (2011).
- ¹¹D.-P. Häder, “Polarotaxis, gravitaxis and vertical phototaxis in the green flagellate, euglena gracilis,” *Archives of microbiology* **147**, 179–183 (1987).
- ¹²M. K. Panda, R. Singh, A. C. Mishra, and S. K. Mohanty, “Effects of both diffuse and collimated incident radiation on phototactic bioconvection,” *Physics of Fluids* **28**, 124104 (2016).
- ¹³M. K. Panda, “Effects of anisotropic scattering on the onset of phototactic bioconvection with diffuse and collimated irradiation,” *Physics of Fluids* **32**, 091903 (2020).
- ¹⁴B. Straughan, *Mathematical aspects of penetrative convection* (CRC Press, 1993).

- ¹⁵R. V. Vincent and N. A. Hill, “Bioconvection in a suspension of phototactic algae,” *Journal of Fluid Mechanics* **327**, 343–371 (1996).
- ¹⁶S. Ghorai and N. A. Hill, “Penetrative phototactic bioconvection,” *Physics of fluids* **17**, 074101 (2005).
- ¹⁷S. Ghorai, M. K. Panda, and N. A. Hill, “Bioconvection in a suspension of isotropically scattering phototactic algae,” *Physics of Fluids* **22**, 071901 (2010).
- ¹⁸S. Ghorai and M. K. Panda, “Bioconvection in an anisotropic scattering suspension of phototactic algae,” *European Journal of Mechanics-B/Fluids* **41**, 81–93 (2013).
- ¹⁹M. K. Panda and R. Singh, “Penetrative phototactic bioconvection in a two-dimensional non-scattering suspension,” *Physics of Fluids* **28**, 054105 (2016).
- ²⁰M. K. Panda, P. Sharma, and S. Kumar, “Effects of oblique irradiation on the onset of phototactic bioconvection,” *Physics of Fluids* **34**, 024108 (2022).
- ²¹S. Kumar, “Phototactic isotropic scattering bioconvection with oblique irradiation,” *Physics of Fluids* **34**, 114125 (2022).
- ²²S. Kumar, “Isotropic scattering with a rigid upper surface at the onset of phototactic bioconvection,” *Physics of Fluids* **35**, 024106 (2023).
- ²³J. R. Cash and D. R. Moore, “A high order method for the numerical solution of two-point boundary value problems,” *BIT Numerical Mathematics* **20**, 44–52 (1980).
- ²⁴S. Kitsunezaki, R. Komori, and T. Harumoto, “Bioconvection and front formation of paramecium tetraurelia,” *Physical Review E* **76**, 046301 (2007).
- ²⁵J. Kessler, “Path and pattern—the mutual dynamics of swimming cells and their environment,” *Comments Theor. Biol.* **1**, 85–108 (1989).
- ²⁶M. K. Panda and S. Ghorai, “Penetrative phototactic bioconvection in an isotropic scattering suspension,” *Physics of Fluids* **25**, 071902 (2013).
- ²⁷N. A. Hill and D.-P. Häder, “A biased random walk model for the trajectories of swimming micro-organisms,” *Journal of theoretical biology* **186**, 503–526 (1997).
- ²⁸A. Kage, C. Hosoya, S. A. Baba, and Y. Mogami, “Drastic reorganization of the bioconvection pattern of chlamydomonas: quantitative analysis of the pattern transition response,” *Journal of Experimental Biology* **216**, 4557–4566 (2013).
- ²⁹N. H. Mendelson and J. Lega, “A complex pattern of traveling stripes is produced by swimming cells of bacillus subtilis,” *Journal of bacteriology* **180**, 3285–3294 (1998).

- ³⁰S. M. Gittleson and T. L. Jahn, “Pattern swimming by polytomella agilis,” *The American Naturalist* **102**, 413–425 (1968).
- ³¹N. S. Khan, T. Gul, M. A. Khan, E. Bonyah, and S. Islam, “Mixed convection in gravity-driven thin film non-newtonian nanofluids flow with gyrotactic microorganisms,” *Results in physics* **7**, 4033–4049 (2017).
- ³²T. Hayat, A. Alsaedi, *et al.*, “Development of bioconvection flow of nanomaterial with melting effects,” *Chaos, Solitons & Fractals* **148**, 111015 (2021).
- ³³F. P. Incropera, T. R. Wagner, and W. G. Houf, “A comparison of predictions and measurements of the radiation field in a shallow water layer,” *Water Resources Research* **17**, 142–148 (1981).
- ³⁴K. J. Daniel, N. M. Laurendeau, and F. P. Incropera, “Prediction of radiation absorption and scattering in turbid water bodies,” (1979).
- ³⁵N. A. Hill, T. J. Pedley, and J. O. Kessler, “Growth of bioconvection patterns in a suspension of gyrotactic micro-organisms in a layer of finite depth,” *Journal of Fluid Mechanics* **208**, 509–543 (1989).
- ³⁶M. F. Modest and S. Mazumder, *Radiative heat transfer* (Academic press, 2021).
- ³⁷S. Chandrasekhar, “Radiative transfer dover publications inc,” New York (1960).
- ³⁸S. Ghorai and R. Singh, “Linear stability analysis of gyrotactic plumes,” *Physics of Fluids* **21**, 081901 (2009).
- ³⁹W. H. Press, “Numerical recipes in fortran.” *The Art of Scientific Computing*. (1992).